the backscattered value. Table 2 summarizes the scattered energies for both back and sidescattering. The total sidescatter energy was calculated by interpolating the angular distribution from $\Theta = 15°$ to $\Theta = 26°$. For the high intensity prepulsed case (A), we find that the total sidescatter energy is approximately 55 percent of the incident compared to 12 percent in the direct backscatter. Above 2 to 3×10^{15} W/cm^2, the Brillouin scattering appears to saturate at the above values [26,27,28].

In summary, these measurements show that for laser plasmas with appreciable density scalelengths, most of the scattered light (out to angles of 60° to the incident beam) can be attributed to the stimulated Brillouin process. Assuming axial symmetry, the energy measurements show that the Brillouin sidescatter can represent more than 50 percent of the incident light.

Table 2
Fraction of scattered energy (%) compared to the incident energy at two different intensities for type (A) pulse. Prepulse energy was kept constant for each intensity.

Laser Intensity	Brillouin Backscatter	Brillouin Sidescatter
3×10^{15} W/cm^2	12 %	52 %
7×10^{15} W/cm^2	12 %	55 %

2.B Progress in Radiationally Cooled Target Experiments

Over the last few months we have extended and refined the measurements of radiationally cooled, Argon filled target implosions. As summarized in the discussion of radiationally cooled targets in Volume 1 of the LLE Review, such implosions lead to highly compressed densities, and the x-ray line spectrum of the Ar^{+16} and Ar^{+17} ions enables a direct determination of core densities and temperatures near the time of peak compression in the implosion event. Densities as high as 6 g/cm^3 and temperatures of about 1 KeV have been measured in this way in our experiments.

The recent set of experiments added a variety of parametric effects to extend our previous results:

1. The effect of different beam focusing conditions on the core compression.
2. The compression of a fill mixture of Argon and thermonuclear fuel rather than just Argon.

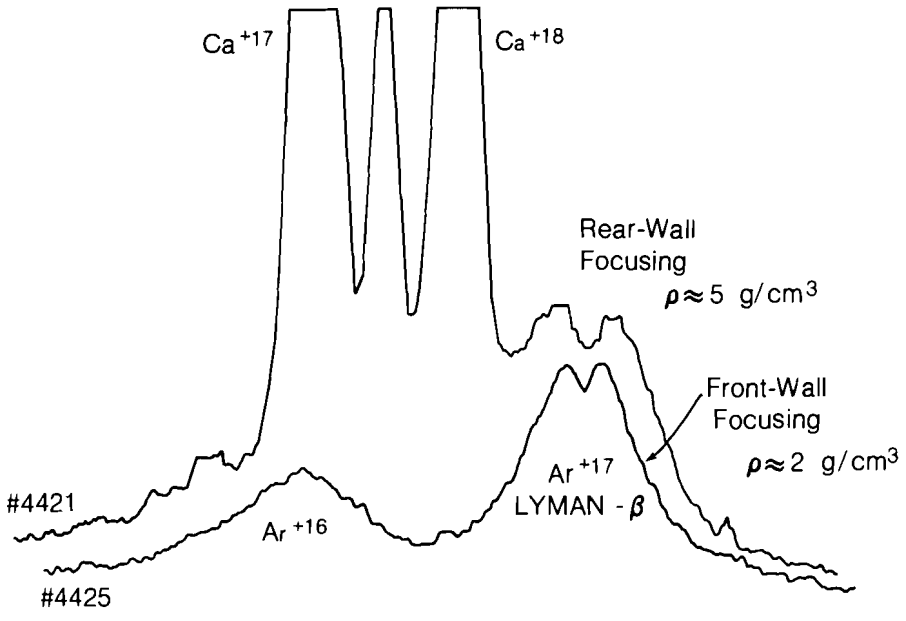

Figure 26
Higher compressed density with better symmetry focusing.

3. Time resolved x-ray measurements of radiationally cooled targets (where the radiation around peak compression decays very fast).
4. Imploding a target of low pressure Argon fill which leads to a high volumetric compression ratio (~1000).
5. Improved (lithographically produced) slits to image the target for each spectral line with a spatial resolution of 7 μm. Such information used with a computer code to perform the required deconvolution enables us to corroborate the determination of density by spectral profiles.

We illustrate below some of the recent results and briefly discuss their significance. The laser and target parameters for the four shots we discuss in these examples are summarized in Table 3. Figure 26 shows that focusing the laser beams on the rear surface of the target produces broader Argon line profiles, indicating a higher peak density, as compared with focusing on the front surface of the target. X-ray imaging (in two dimensions)

Table 3
Laser and target parameters for the shots used as examples in Figures 25 through 30. +2R focusing means two target radii behind center.

Shot Number	Absorbed Laser Energy (J)	Pulse Width (psec)	Focusing W/r to Center	Target Diameter (μm)	Wall Thickness (μm)	Plastic Coating (μm)	Ar Fill Pressure (atm)
4421	35	68	+1R	50	1.65	2.5	50
4425	47	87	-1R	46	1.40	2.8	50
4429	32	75	+2R	47	2.30	2.5	50
4436	35	65	+1R	47	1.86	3.5	3

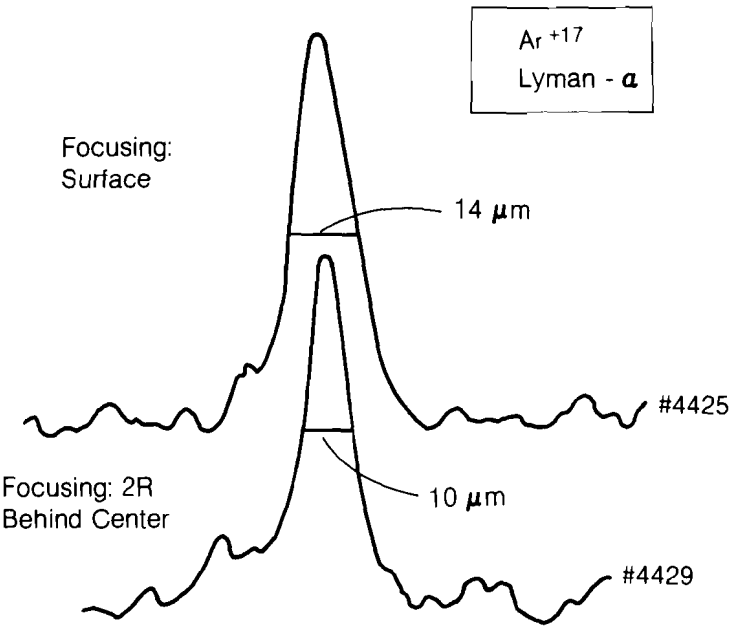

Figure 27
Smaller compressed Argon core achieved with higher symmetry focus.

shows that better spherical symmetry is achieved in the former case. These results demonstrate that better symmetry leads to higher compression.

Figure 27 shows that focusing two target radii behind the target center (which, as judged by x-ray pinhole photographs, yields best symmetry of illumination) leads to a smaller compressed core as compared with focusing on the front surface of the target. The curves in Figure 27 pertain to a single Ar^{+17} line (the 2→1 transition at 3.321 KeV) as a function of a spatial (lateral) coordinate.

Figure 28 compares the spectrum in the range of 3-4 KeV for two focusing conditions: (a) two radii being the center, and (b) rear surface. One striking difference between the two is in the intensity ratios between the two Argon resonance lines at 3.140 keV and 3.321 keV and with the nearby dielectronic satellite lines marked S. The explanation of these differences is that the target in shot no. 4429 is compressed to a higher ρR. The higher ρR leads to a higher intensity of Argon lines which is clearly evident for the S lines. However, the resonance lines (of the Ar^{+16} and Ar^{+17} ions) do not increase because of saturation which is characteristic of heavily absorbed resonance lines. Another striking difference between the two spectra of Figure 28 is the severe attenuation of Ca^{+18} lines in going from the lower to the upper spectrum in the figure. This indicates a significantly lower temperature in shot no. 4429. It is characteristic of radiationally cooled targets that higher density is caused by (and in turn is causing) a lower temperature.

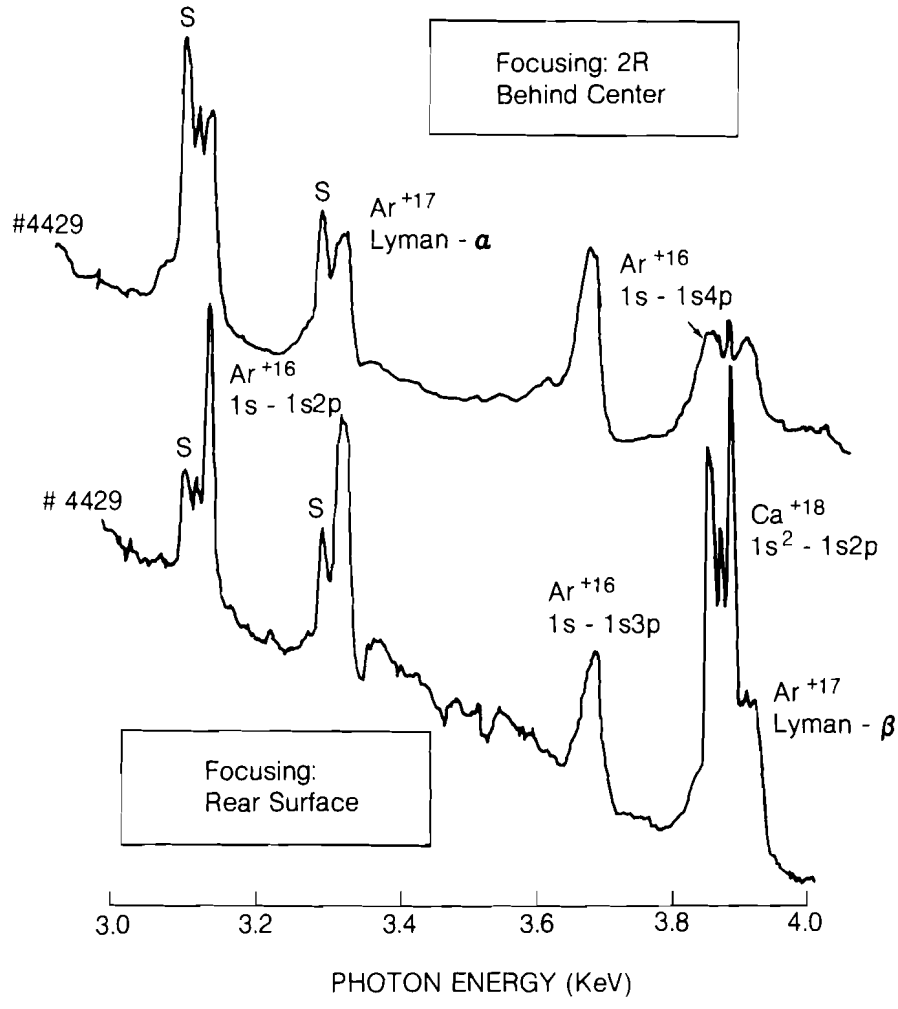

Figure 28
Higher ρR and increased radiation cooling in higher symmetry focusing.

Figures 29 and 30 show parts of the spectrum for a target of 3 atmosphere fill pressure of Argon (this fill is lower than most other target shots in this series). The Stark-broadened profile of the Ar^{+17} Lyman-β line (3→1) indicates a compressed core density of 5 g/cm³. If the whole Ar fill gas were compressed, this would indicate a volumetric compression ratio of 1020 which corresponds to a size of the compressed Argon region of 4.5 microns. To corroborate this, we show in Figure 31 a one-dimensional image of the target at the Lyman-β line radiation obtained with a resolving slit of width 6μm. The lower scan is taken at a spectral position off the Argon line, and it shows the continuum radiation which has to be subtracted from the upper curve to obtain the net radiation of Argon. In doing so, it is clear that we should get a small emission region whose image is limited by the slit resolution. The results thus provide an indication, but not a proof, of the validity of the high compression deduced from the spectral profile of Figure 30.

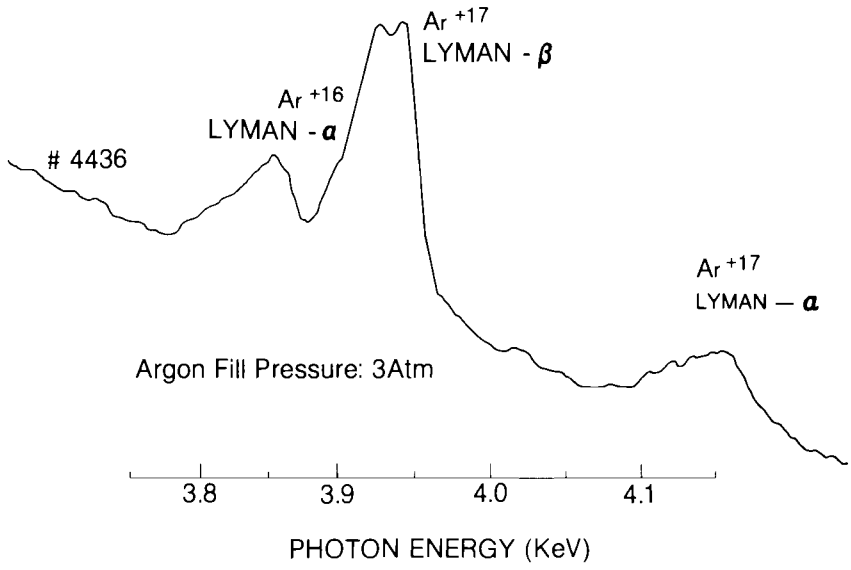

Figure 29
Asymmetry of Lyman-β Stark profile in low Argon fill pressure implosion.

Finally, an interesting feature in Figures 29 and 30 is the asymmetry of the Lyman-β profile: The higher energy peak is more intense than the lower energy peak. This is particularly evident when we consider that the underlying continuum rises for lower energies (see Figure 29). This asymmetry, not currently accounted for by the theory of Stark broadening, is thought to be caused by shielding of the nucleus from the radiating electron by neighboring electrons of the plasma. This effect, thought to exist in very high density plasmas is now under active study.

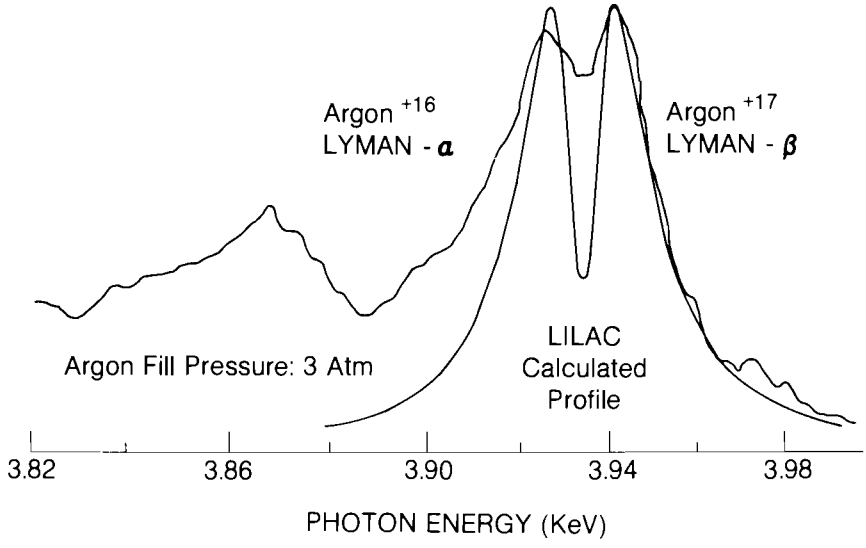

Figure 30
High density and asymmetric Lyman-β profile low Argon fill pressure implosion.